Aerosol and Air Quality Research, 16: 2742–2756, 2016

ISSN: 1680-8584 print / 2071-1409 online
doi: 10.4209/aaqr.2015.07.0447

Investigation of the CCN Activity, BC and UVBC Mass Concentrations of Biomass Burning Aerosols during the 2013 BASELInE Campaign

Ta-Chih Hsiao[1*], Wei-Cheng Ye[1], Sheng-Hsiang Wang[2], Si-Chee Tsay[3], Wei-Nai Chen[4], Neng-Huei Lin[2], Chung-Te Lee[1], Hui-Ming Hung[5], Ming-Tung Chuang[6], Somporn Chantara[7]

[1] *Graduate Institute of Environmental Engineering, National Central University, Chung-Li 32001, Taiwan*
[2] *Department of Atmospheric Sciences, National Central University, Chung-Li 32001, Taiwan*
[3] *Goddard Space Flight Center, NASA, Greenbelt, Maryland, USA*
[4] *Research Center for Environmental Changes, Academia Sinica, Taipei 11529, Taiwan*
[5] *Department of Atmospheric Sciences, National Taiwan University, Taipei 10617, Taiwan*
[6] *Graduate Institute of Energy Engineering, National Central University, Chung-Li 32001, Taiwan*
[7] *Environmental Science Program, Chiang Mai University, Chiang Mai, Thailand*

ABSTRACT

Biomass-burning (BB) aerosols, acting as cloud condensation nuclei (CCN), can influence cloud microphysical and radiative properties. In this study, we present CCN measured near the BB source regions over northern Southeast Asia (Doi Ang Khang, Thailand) and at downwind receptor areas (Lulin Atmospheric Background Station, Taiwan), focusing exclusively on 13–20 March 2013 as part of 2013 spring campaign of the Seven SouthEast Asian Studies (7-SEAS) intensive observation. One of the campaign's objectives is to characterize BB aerosols serving as CCN in SouthEast Asia (SEA). CCN concentrations were measured by a CCN counter at 5 supersaturation (SS) levels: 0.15%, 0.30%, 0.45%, 0.60%, and 0.75%. In addition, $PM_{2.5}$ and black carbon mass concentrations were analyzed by using a tapered element oscillating microbalance and an aethalometer. It was found the number-size distributions and the characteristics of hygroscopicity (e.g., activation ratio and κ) of BB aerosols in SEA have a strong diurnal pattern, and different behaviors of patterns were characterized under two distinct weather systems. The overall average κ value was low (0.05–0.1) but comparable with previous CCN studies in other BB source regions. Furthermore, a large fraction of UV-absorbing organic material (UVBC) and high Delta-C among BB aerosols were also observed, which suggest the existence of substantial particulate organic matter in fresh BB aerosols. These data provide the most extensive characterization of BB aerosols in SEA until now.

Keywords: Cloud condensation nuclei; Biomass burning aerosol; Long-range transport; Diurnal cycle; Hygroscopicity.

INTRODUCTION

Biomass-burning (BB) activity is a major contributor to global fine particles and particle precursors (Crutzen and Andreae, 1990; Andreae *et al.*, 2004; Aiken *et al.*, 2010). BB aerosols have gained attention because of their significant role on modulating Earth's radiation budget and their contribution to the uncertainty of the aerosol effect on climate change (Bates *et al.*, 2006). In addition to aerosol's direct radiative effects, such as backscattering and absorption of solar radiation (Bhawar and Rahul, 2013; Wang *et al.*, 2015; Sayer *et al.*, 2016; Pani *et al.*, 2016a, b), BB aerosols also have indirect influence on the radiation budget and the regional water cycle by acting as cloud condensation nuclei (CCN). Activation of aerosol particles as CCN is a crucial factor for the dynamical and microphysical evolution of clouds (Andreae and Rosenfeld, 2008; Adesina *et al.*, 2016). Model simulations have demonstrated that BB aerosols are a major global source of CCN (Pierce *et al.*, 2007; Spracklen *et al.*, 2011).

The main parameters governing CCN activation and initial cloud droplet growth are the number, size, and hygroscopicity of aerosol particles, as well as updraft velocity at the cloud base and the resulting water vapor supersaturation (*SS*) (Reutter *et al.*, 2009). In other words, CCN activity revealed in terms of Activation Ratio (*AR*) is strongly related to the physical and chemical properties of aerosols (Martin, 2000). AR is the ratio of the number concentrations of CCN ($N_{CCN}(SS)$) to CN (N_{CN}) at different *SS* levels. The number fraction of CN activated to CCN at a specific *SS* (*AR*(*SS*)) is determined as:

* Corresponding author.
E-mail address: tchsiao@cc.ncu.edu.tw

$$AR(SS) = \frac{N_{CCN}(SS)}{N_{CN}}. \quad (1)$$

Petters and Kreidenweis (2007) proposed a simple way to describe the effect of chemical composition on the CCN activity, κ, which is based on the Köhler theory.

$$\kappa = \frac{4A^3}{27D_{act}(SS)^3 ln^2 SS}$$
$$\mathrm{A} = \frac{4\sigma_{s/a}M_W}{RT\rho_W} \quad (2)$$

where M_w is the molecular weight of water, $\sigma_{s/a}$ is the surface tension of the interface between the solute and air, R is the universal gas constant, T is temperature, and ρ_w is the density of water. The activation diameter (D_{act}) for a specific SS value can be estimated:

$$\frac{\int_{D_0}^{D_{act}(SS)} N(D)dD}{N_{CN}} = 1 - AR(SS), \quad (3)$$

where $N(D)$ is the dry particle size distribution (PSD), and D_0 is the lower bound of the dry PSD.

Previous field and laboratory studies on BB aerosols have found that their properties are directly related to their biomass materials, combustion phase, and degree of aging status (Reid *et al.*, 2005). Early laboratory studies conducted by Hallett *et al.* (1989) and Dinh *et al.* (1992) showed that the CCN's AR of BB aerosols from flame burning is higher than that from smoldering. Wardoyo *et al.* (2007) and Reid *et al.* (2005) reported that the count-median-diameter (CMD) of particles produced from flame burning is larger than that from smoldering and suggested that size is an important factor for CCN activation. On the other hand, Carrico *et al.* (2010) attributed the difference in CCN activation ratios of flaming and smoldering aerosols to their different chemical compositions. In their laboratory work, smoldering aerosols have a relatively low κ value and a higher mass fraction of organic carbon. Furthermore, the type of biomass fuel could greatly influence CCN activity. Petters *et al.* (2009) experimentally observed a high variation of activity of CCN in BB aerosols emitted from 24 different biomass materials. They reported that the κ value can vary from 0.02 (weak hygroscopicity) to 0.8 (high hygroscopicity).

For field study near BB source regions, Lathem *et al.* (2013) conducted flight measurements and showed that fresh BB aerosols had a CCN's AR (AR = 0.89, SS = 0.55%) higher than the aged BB ones (AR = 0.35, SS = 0.55%). However, the latter had a higher κ value (0.24 ± 0.10) than that for the former (0.11 ± 0.04). A smaller range of particle size distributions explained the lower CCN activation ratio of aged BB aerosols, which was a result of wet-deposition loss and heterogeneous chemical reactions during transport. On the other hand, Pratt *et al.* (2011) showed that fresh BB aerosols contained a lower mass fraction of hygroscopic materials such as sulfate and nitrate, which increase with aging. Therefore, the increase in hygroscopicity of CCN in aged BB aerosols is expected. Engelhart *et al.* (2012) reported a chamber study for simulating the aging process of BB aerosols by exposing it to UV light. The κ value prior to photochemical aging varied widely (between 0.06 and 0.6), whereas it converged to 0.2 ± 0.1 within a few hours of exposure to UV light. This change is attributed to the formation of secondary organic aerosol (SOA), which has low hygroscopicity (κ = 0.11). All of the aforementioned experimental results and field observations showed the complexity and capabilities of BB aerosols acting as CCN, and also revealed the need to characterize further BB aerosols in both BB source regions and receptor areas.

Most of the reported ground or flight measurements on BB aerosols were performed in Africa (Anderson *et al.*, 1996; Le Canut *et al.*, 1996; Haywood *et al.*, 2003; Posfai *et al.*, 2003), North America (Levine 1996; Clarke *et al.*, 2007), and South America (Anderson *et al.*, 1996; Reid and Hobbs, 1998). The previous studies more focused on physical, chemical and optical properties of BB aerosol (Heil and Goldammer, 2001; Corrigan *et al.*, 2006; See *et al.*, 2006) but very few studies investigated the CCN activity in SEA, which is considered as one of the major source regions in the world of biomass-burning activities (Duncan *et al.*, 2003; Streets *et al.*, 2003). The 2013 7-SEAS/BASELInE (Seven SouthEast Asian Studies/Biomass-burning Aerosols & Stratocumulus Environment: Lifecycles and Interactions Experiment) (Tsay *et al.*, 2013; Lin *et al.*, 2014) campaign has been the most extensive campaign for characterizing the physical and chemical properties of BB aerosols in SEA. This study was part of the 2013 spring 7-SEAS/BASELInE campaign (Tsay *et al.*, 2016) that the PSD and characteristics of hygroscopicity (e.g., AR, D_{act}, κ) of BB aerosols in SEA near the source regions are presented. $PM_{2.5}$, and black carbon (BC) mass concentrations were also measured. All of the measurements we report herein were performed on 13–20 March 2013, which falls within the dry season in Thailand, during which BB events are serious. No previous studies on particle number-size distributions and CCN characteristics have yet been made in SEA, as well as comparing the different levels of hygroscopic ability near the source regions and receptor areas.

METHODS

Observation Sites

Experiments were conducted at two different sites, namely, the Doi Ang Kang meteorology Station (DAK; 19.93°N, 99.05°E, 1536 m above sea level) and the Lulin Atmospheric Background Station (LABS; 23.47°N, 120.87°E, 2862 m a.s.l.), as shown in Fig. 1. Data collected at both sites covering the period from 1 March to 8 April 2013. DAK is located in the northern part of Thailand and is close to the border between Thailand and Myanmar, in which the local residents annually burn fields in the area to clear it for agriculture during the dry season from late February to mid-April. DAK is an excellent site for investigating the characteristics of BB aerosols near the source regions. Located at the middle of Taiwan, LABS is a high-elevation

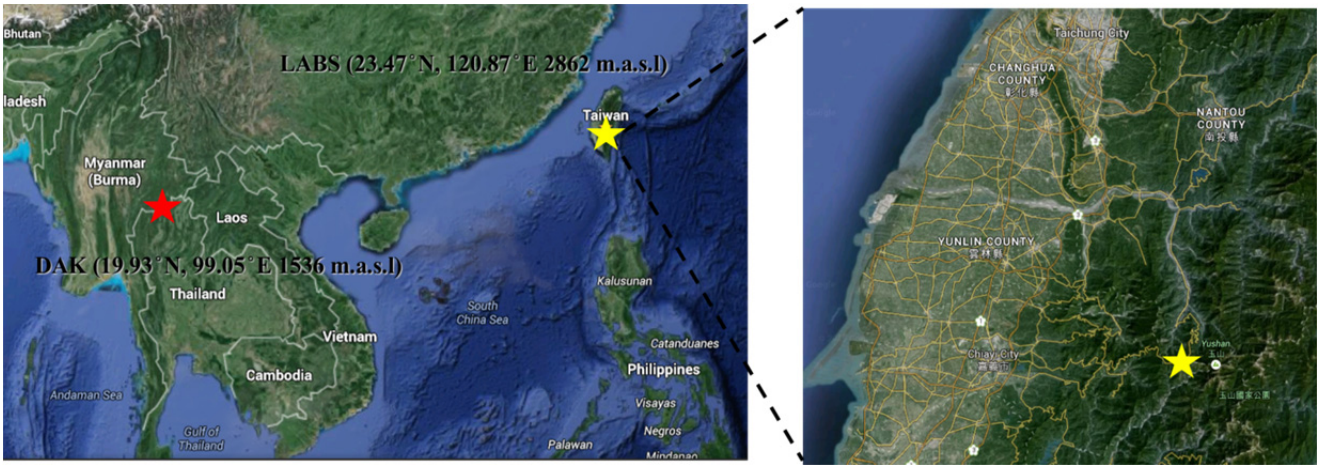

Fig. 1. Sampling locations of DAK and LABS. The distance from DAK to LABS is ~2000 km.

baseline station in East Asia. With the main traffic roads ~2 km away, the high altitude of LABS in the free-troposphere avoids direct influence of local pollutions.

In this study, the time of 13–20 March 2013 was selected as "golden days" for detailed data analyses as DAK was affected by two different weather systems in the early and late stages of this period. During March 13 to 16, the prevailing wind changed from northerly to southwesterly, with wind speed of about 2–5 m s^{-1}, which implies DAK was at junction of different weather systems. Weather maps (*cf.* Fig. S1) also indicate that DAK was covered by a low-pressure system on March 12. A Siberian–Mongolian high-pressure cell over China moved southwardly and countered DAK on March 13. During March 14 and 15, DAK was on the edge of a high-pressure system. On March 15 one low pressure in the north moved toward DAK and covered on DAK from March 16 to 19. The prevailing wind was southwesterly with higher wind speed about 5–10 m s^{-1} during the late period.

Instrumentation

NASA's SMART (Surface-sensing Measurements for Atmospheric Radiative Transfer, *cf.* http://smartlabs.gsfc.nasa.gov) mobile laboratory was deployed at DAK for remote sensing and *in-situ* measurements. In addition, SMART also hosted various aerosol microphysics probes from National Central University in Taiwan. As shown in Fig. 2, the inlets are 2 meters above the roof of a sea container. Total height is 4.5 meters. The day time RH of ambient air measured during the campaign was about 40%. Instruments zero-air test length and intercomparison tests completed before, during and after the campaign are listed in Table S1. CCN activity was measured by two different systems: a cloud condensation nuclei counter (CCNc) and a scanning mobility particle sizer (SMPS). The CCNc (CCN-100, Droplet Measurement Technologies) utilizes thermal-gradient technique to quantify the CCN concentration at different supersaturation levels and was operated at 0.5 L min^{-1}. The ambient dry PSD were measured by using a SMPS (model 3936, TSI) composed of an electrostatic classifier (3080, TSI), a differential mobility analyzer (3081, TSI), and a water-based condensation particle counter (CPC; 3787, TSI). The SMPS was operated at sheath flow of 3.0 and aerosol flow of 0.6 L min^{-1} to obtain the size range of 13.3 to 749.9 nm. The mass concentration of $PM_{2.5}$ was measured by using a tapered element oscillating microbalance (TEOM; 1400a, R&P Inc.) with its sampling flow heated to 50°C to remove water and semivolatile species. An aethalometer (AE31, Magee) was used to estimate the BC mass concentration at a flow rate of 4.0 L min^{-1}. The receptor site, LABS, had two aerosol measurement systems. One is a long-term observation system composed of a CPC (3010, TSI), a TEOM (1400a, R&P) and an aethalometer (AE-31, Magee). The other is an intensive-observation-period (IOP) system, employed at a certain observation period, included a CCNc (CCN-100, Droplet Measurement Technologies) and a SMPS composed of an electrostatic classifier (3080, TSI), a differential mobility analyzer (3081, TSI), and a butanol-based CPC (3010, TSI).

Data Processing and Analysis

The CCN concentration for each of the five SS levels (0.15%, 0.30%, 0.45%, 0.60%, and 0.75% for DAK; 0.14%, 0.21%, 0.28%, 0.42%, and 0.57% for LABS) was measured for 12 min. Data points of the first and last two minutes were discarded because of the unstable temperature gradient. SMPS was operated for a 240 sec upscan and a 60 sec downscan at a sampling cycle of 6 min. Each data point from the TEOM and AE-31 was recorded every 30 and 5 min, respectively. Data resolutions of all instruments at both DAK and LABS were identical, and the reported data were adjusted and averaged to a 1 hr time resolution for further data analysis.

RESULTS AND DISCUSSION

Time Series of CN Concentration, Geometric Mean Diameter (GMD), and CCN Activity

Fig. 3 illustrates the time series of CCN, CN concentration, and the GMD of CN size distribution at DAK. During the one-week IOP from March 13 to 20 in 2013, the CN concentration varied from as low as 4898 # cm^{-3} to 40767

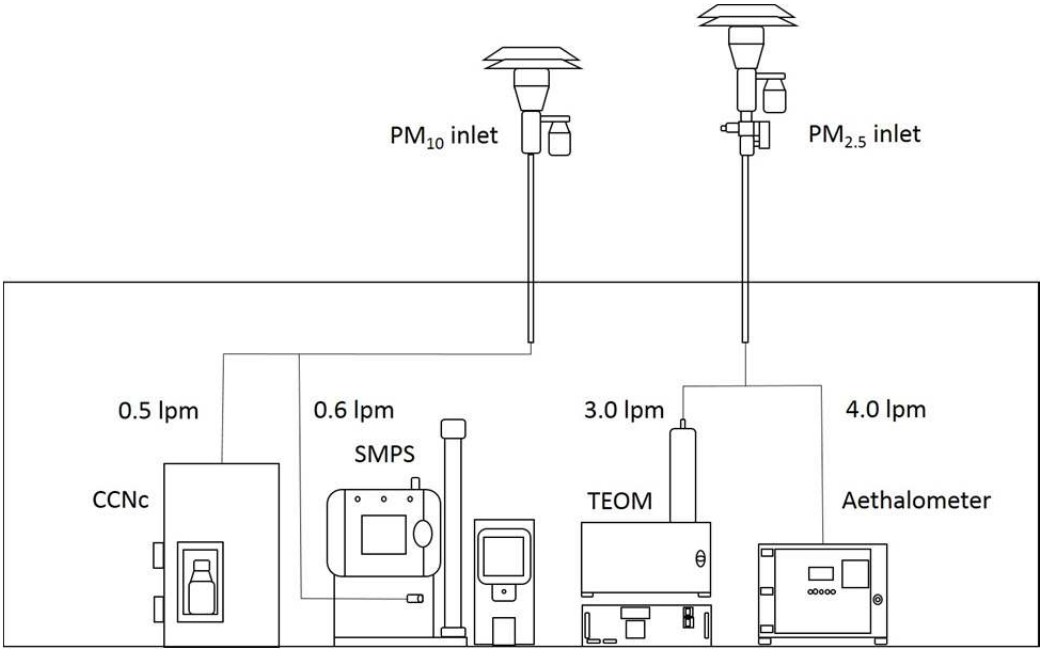

Fig. 2. Schematic diagram of the sampling setup in DAK.

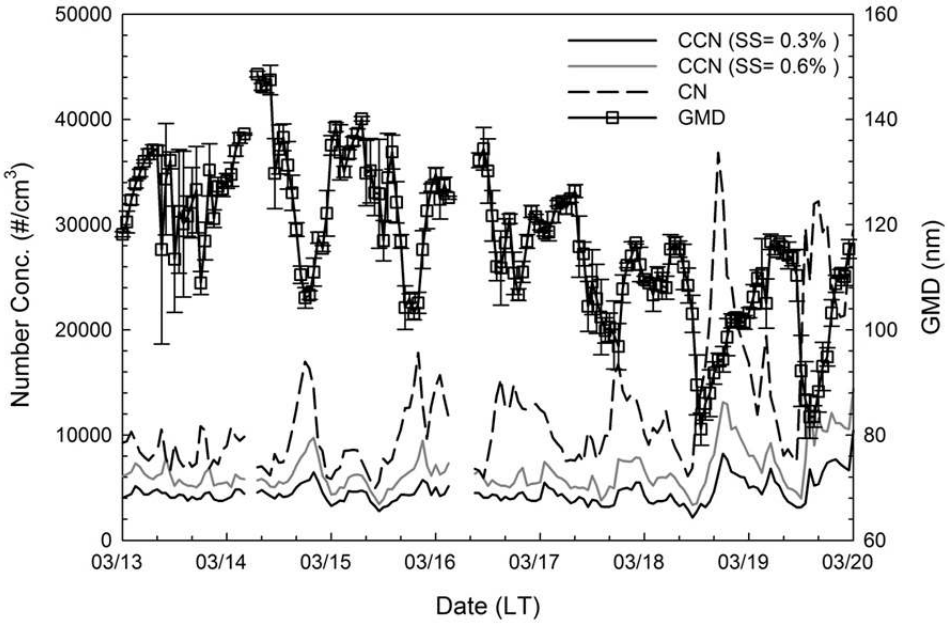

Fig. 3. Time series of CN, CCN number concentrations (SS = 0.3%, 0.6%), and geometric mean diameter (GMD) obtained at DAK.

cm^{-3}, and the average value with one standard deviation was 13566 ± 6899 # cm^{-3}. For the BB aerosols in the Amazon region, the average CN concentration reported by Rissler *et al.* (2006) was 10440 ± 6570 # cm^{-3}, which is about the same magnitude of what have been observed in this study. As seen in the figure, the CN concentration before March 17 was relatively stable (in the order of 10^4) and starts to gradually rise up after that. Meanwhile, the overall GMD gradually decreased as the CN increased because of an increase in CN concentration in the BB source region. It is because, near the BB source region, the rise of CN concentration potentially indicates the increasing of number of neighboring fire events, which is evidenced by the fire counts recorded by Terra and Aqua (Fig. S2). In addition, the small GMD values also reflect the "freshness" of the measured BB aerosols. However, the daily minimum GMD did not always correspond to the daily maximum CN concentration. For example, at 17:00 p.m. on March 18, the CN concentration reached the maximum value of 36845 # cm^{-3}, while the GMD (94.3 nm) was slightly higher than the daily minimum GMD of 81.1 nm at noon. This phenomenon is attributed to the partial coagulation of

particles resulting from the high BB aerosol concentration from the burning events. In the intensive review of BB aerosols by Reid *et al.* (2005), many studies have found that the size of BB aerosols increase significantly within 30 to 90 min after emission because of particle coagulation. The particle coagulation rate is affected by several environmental factors such as temperature and ambient pressure, as well as particle size and concentration (Reid *et al.*, 2005). Reid *et al.* (1998) further identified the particle growth rate due to coagulation is about 10 nm/45 min for BB aerosols with a concentration of 1.5×10^5 # cm^{-3} in Brazil. When the concentration drop down to 5000–10,000 # cm^{-3}, the growth rate drastically dropped to ~15–30 nm day^{-1}. In addition, the minimum and maximum GMD recorded in DAK after March 17 were 81.1 nm and 126.0 nm respectively, which were just very close to the CMDs of fresh and aged BB aerosols (83 ± 13 nm and 127 ± 6 nm, respectively) measured by Wardoyo *et al.* (2007) in Northern Territory, Australia. The behavior of the time series curves for CCN concentrations in DAK was similar to that of the time series curves for CNs. Maximum values recorded when SS = 0.3% and 0.6% were 8245 and 13132 # cm^{-3}, respectively, and also occurred around 17:00 p.m. on March 18. In addition, the average values with one standard deviation are 4754 ± 1392 # cm^{-3} (SS = 0.3%) and 6821 ± 2271 # cm^{-3} (SS = 0.6%). Fig. 4 shows the time series curves of CCN ARs in DAK. Throughout the week, the average ARs when SS = 0.3% and 0.6% were 0.40 ± 0.13 and 0.56 ± 0.16, respectively. Although the maximum CCN concentration was attained on March 18, the corresponding AR was minimal. Moreover, we observed that the overall trend of the AR gradually decreased and was somewhat similar to the trend of GMD shown in Fig. 3. This decrease may reveal that the BB aerosol was relatively "fresh", and the fresh BB aerosols generally have low hygroscopicity (Andreae and Rosenfeld, 2008; Engelhart *et al.*, 2012; Lathem *et al.*, 2013). Nevertheless, the AR of BB aerosols can be affected by the BB materials and combustion conditions as well (Hallett *et al.*, 1989; Dinh *et al.*, 1992). Fig. S3 shown the timeseries of $PM_{2.5}$ and BC mass concentration, and the average of $PM_{2.5}$ and BC during whole observation was 71.36 and 5.43 μg m^{-3}.

The observed aging (or transport) and freshness of BB aerosols during the sampling period can be further inferred from satellite measurements. Figs. 5(a) and 5(b) show 4 days composed MODIS (Moderate Resolution Imaging Spectroradiometer) aerosol optical depth (AOD) data and wind streamlines for the periods of March 13–16 and March 17–20, respectively, while AOD data is composed from MODIS Terra and Aqua and wind data (10 m) from ECMWF (European Centre for Medium-Range Weather Forecasts). As mentioned above, DAK was on the edge of a high-pressure system during March 14–15. Shown in Fig. 5(a), DAK was located on the eastern edge of a regionally distributed aerosol mass centered at southern Myanmar, with a maximum AOD of ~1.5. The prevailing wind in DAK revealed westerly from the massive aerosols in south Myanmar, which implies that aerosols observed during March 13–16 in DAK were possibly mixed with aging aerosols transported from outside of DAK. Fig. 5(b) shows AOD around DAK region is relatively lower (~0.8) than AOD outside DAK in March 17–20, which implies there was no significant aerosol source near DAK and the observed aerosols were mainly locally produced. These implications consist with the conclusions inferred from GMD and AR analysis.

Diurnal Variation of CN Concentration, GMD, BC Mass Concentration, and CCN Activity in DAK

The CCN activity, GMD, and CN concentration of BB

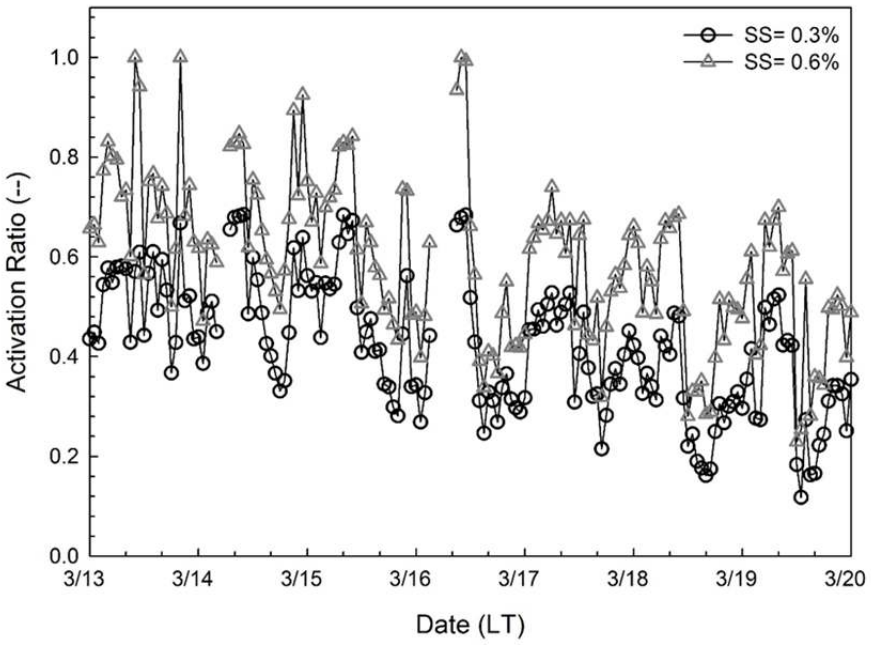

Fig. 4. Time series of activation ratio (SS = 0.3%, 0.6%) obtained at DAK.

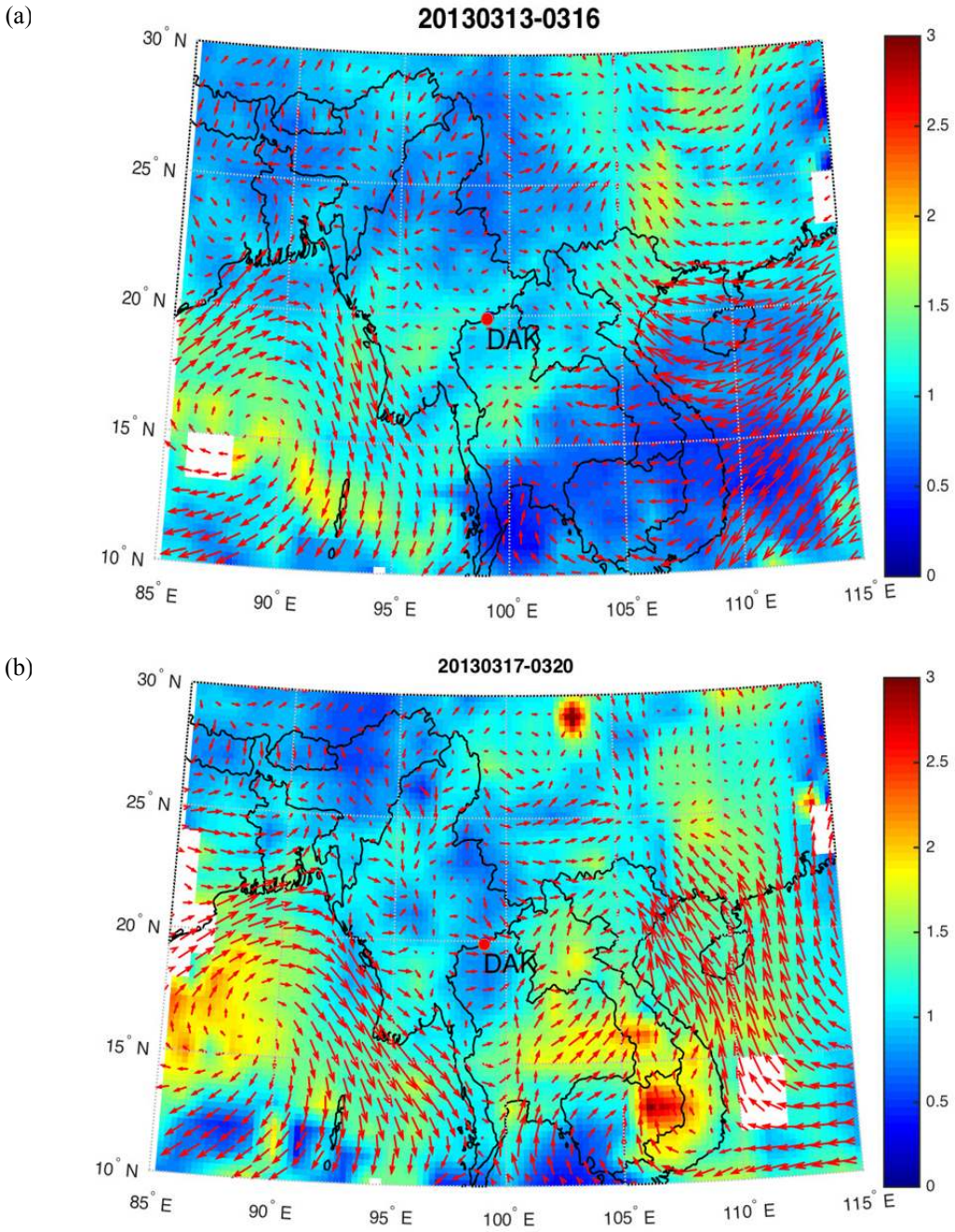

Fig. 5. Four-day MODIS AOD data and wind streamlines for (a) March 13–16 and (b) March 17–19. Wind streamlines are averaged 10 m wind data from ECMWF.

aerosols in DAK showed a strong diurnal cycle during the observation period. As seen in Fig. 6(a), the AR in the morning was generally high (0.6–0.8 at SS = 0.6%) and reached a peak value before noon. AR gradually then decreased and approached a minimum of 0.4–0.5 (SS = 0.6%) at about 17:00 to 18:00. This pattern correlates with the pattern of the GMD (R^2 = 0.472), while it behaves oppositely to the pattern for CN illustrated in Fig. 6(b). The observed diurnal patterns of the AR, GMD, and CN concentration are mainly due to cyclic local burning behavior, boundary layer thickness, and local wind profile. According to the fire-count data monitored by Terra and Aqua (*cf.* Fig. S2), the number of fire events in the afternoon is always higher than that in the morning. This behavior directly supports the observed higher CN concentration and a smaller GMD in the afternoon. On the other hand, the boundary layer descends in the evening. Therefore, the CN concentration drops marginally and stays at ~9000 # cm^{-3} during midnight even though the number of fire events decrease at night. In the early morning, the thickness of the boundary layer starts to expand as the ambient temperature increases, resulting in dilution and a decrease in CN concentration. In summary, the diurnal pattern of CCN activity, GMD, and CN concentration from noon to about

18:00 were mainly influenced by fire counts, and the effect of boundary layer elevation became dominant during the night and in the early morning. Furthermore, the cyclic pattern of wind velocity suggests a potential scenario in which enormous amounts of fresh BB aerosols generated in the afternoon travels downstream and low wind speed during the night induces the local accumulation of BB aerosols. Therefore, the BB aerosols measured in the morning could include part of the BB aerosols generated locally on the day before. The aging process proceeds at night, and part of the aged BB aerosols travels from other upstream BB source regions. At the same time, the diurnal pattern of BC mass concentration and BC/$PM_{2.5}$ ratio is relatively flat (Fig. 6(c)), also implying that the BB aerosols measured before March 17 constituted local fresh BB aerosols and is partially mixed with the transported or aged BB aerosols.

Similar patterns of CCN activity, GMD, and CN concentration were observed in the diurnal cycles after March 17 (Figs. 6(d)–6(f)). The correlation between GMD and AR was high. The linear R^2 could increase up to 0.708. However, the AR value was smaller and the CN concentration was higher than those observed before March 17. In comparison

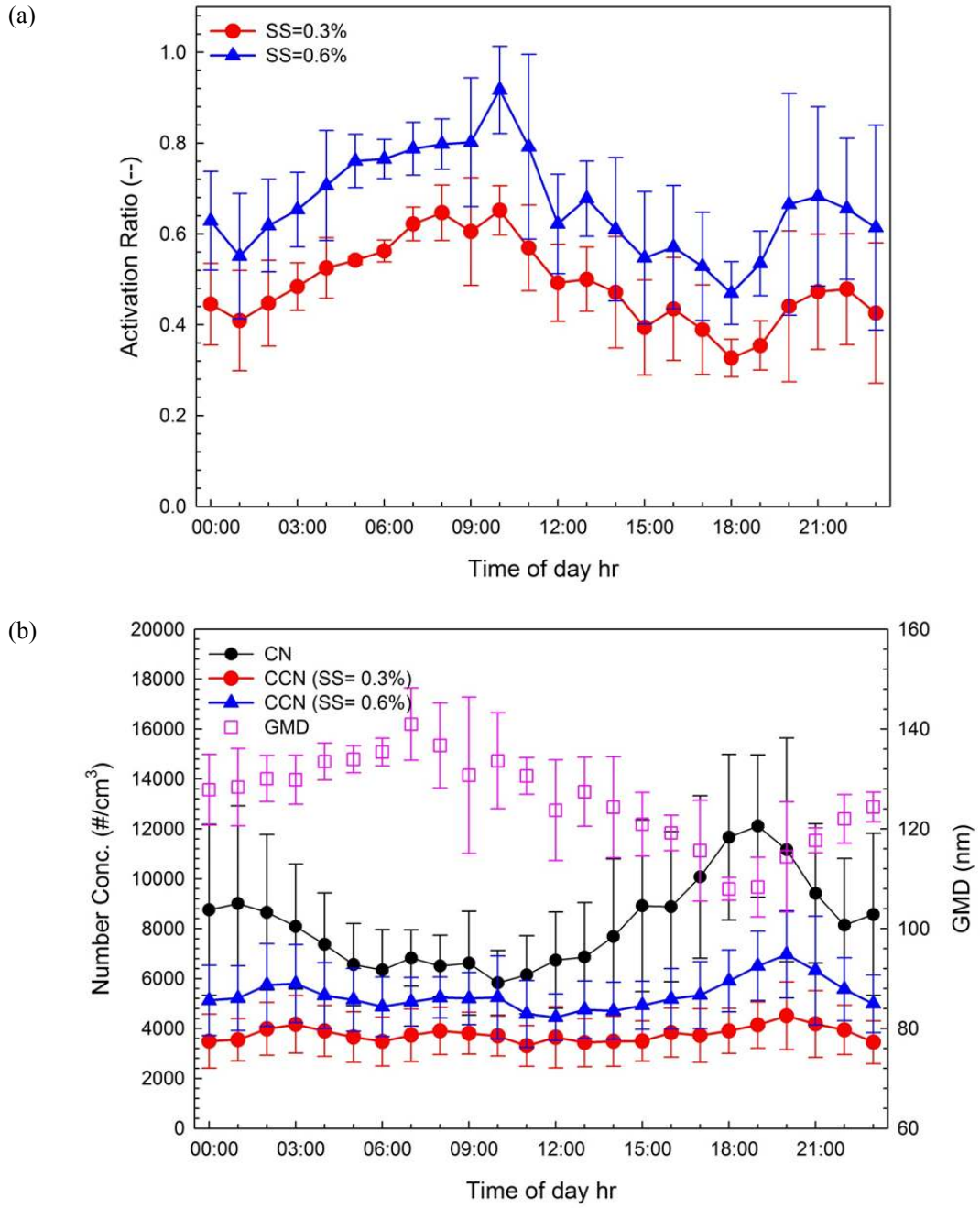

Fig. 6. Diurnal patterns of (a) activation ratio (SS = 0.3%, 0.6%) during March 13–16; (b) CN, CCN (SS = 0.3%, 0.6%), and GMD during March 13–16; (c) BC and BC/$PM_{2.5}$ during March 13–16; (d) activation ratio (SS = 0.3%, 0.6%) during March 17–19; (e) CN, CCN (SS= 0.3%, 0.6%), and GMD before March 17–19; and (f) BC and BC/$PM_{2.5}$ during March 17–19.

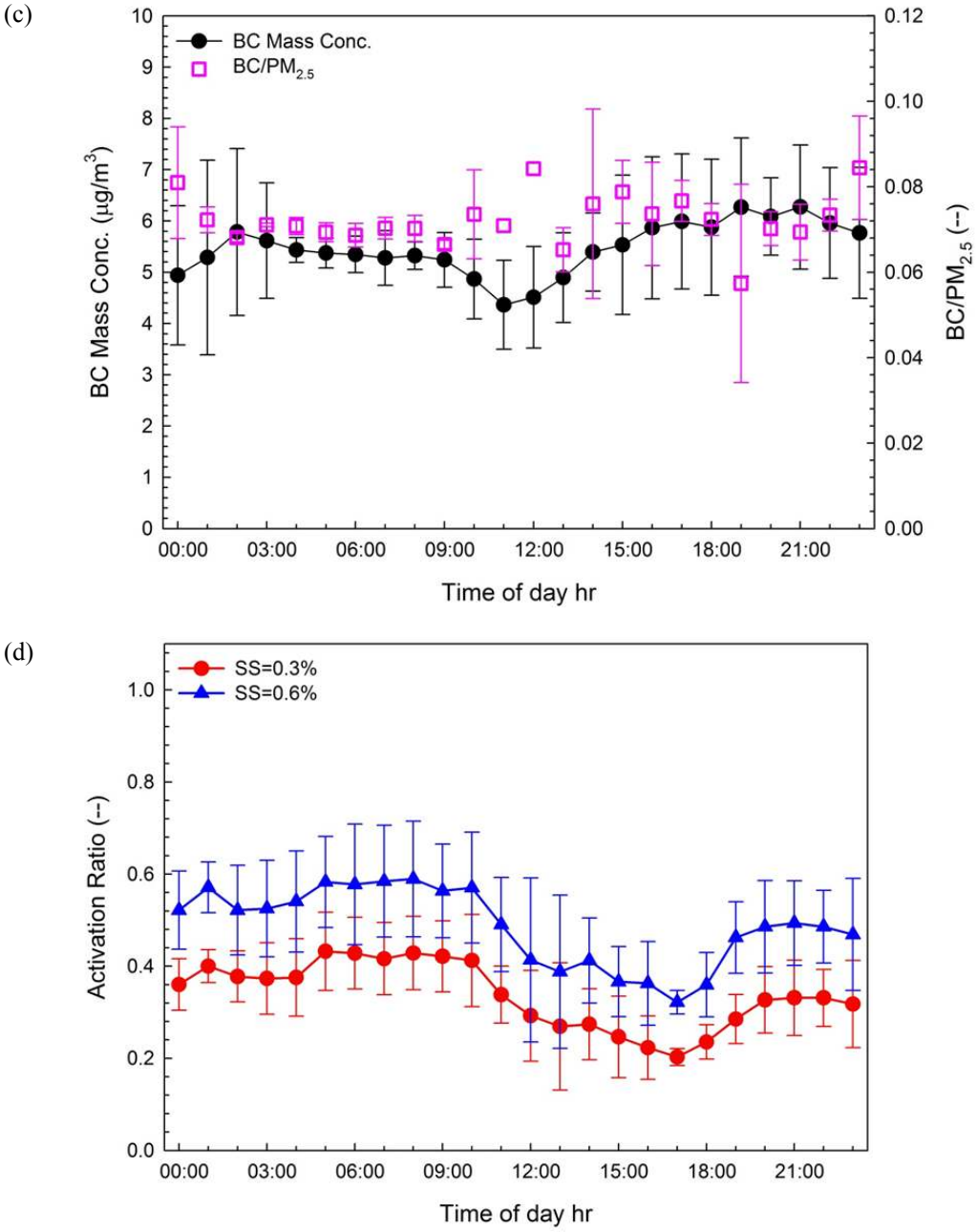

Fig. 6. (*continued*).

with the patterns before March 17, both the CN and GMD diurnal patterns showed a steeper change (Fig. 6(e)). The minimum GMD lowered to 89 nm, and the nadir occurred earlier at noon. These phenomena thus also demonstrated that the BB aerosols measured after March 17 was relatively fresh.

Previous studies using aethalometer measurements have suggested that certain organic aerosol components such as aromatic organic species of wood smoke or BB aerosols have enhanced UV absorption at 370 nm, relative to that at 880 nm (Jeong *et al.*, 2004; Park *et al.*, 2006; Sandradewi *et al.*, 2008; Kumar *et al.*, 2011; Wang *et al.*, 2011; Yu *et al.*, 2014). Therefore, the ratio between BC concentrations measured at wavelengths of 880 nm (BC_{880nm}) and 370 nm (BC_{370nm}), also known as UVBC, as well as the Delta-C value ($BC_{370nm}-BC_{880nm}$) were calculated and plotted in Fig. 7. Yu *et al.* (2014) reported that the slope of the equation for the regression between BC_{370nm} and BC_{880nm} is 0.95 for the non-BB period and 1.29 for the BB period, which correspond to BC_{880nm}/BC_{370nm} values of 1.05 (non-BB) and 0.77 (BB) here. As seen in Fig. 7, the BC_{880nm}/BC_{370nm} for the entire observation period was always less than 1.0, and the mean ratio during March 17–19 further dropped to 0.72 ± 0.05. The mean Delta-C values, a qualitative indicator for biomass smoke, after March 17 are almost double the mean value before March 17 and demonstrated a wider diurnal variation. These results indicate that stronger BB events or fresher BB aerosols were measured on March

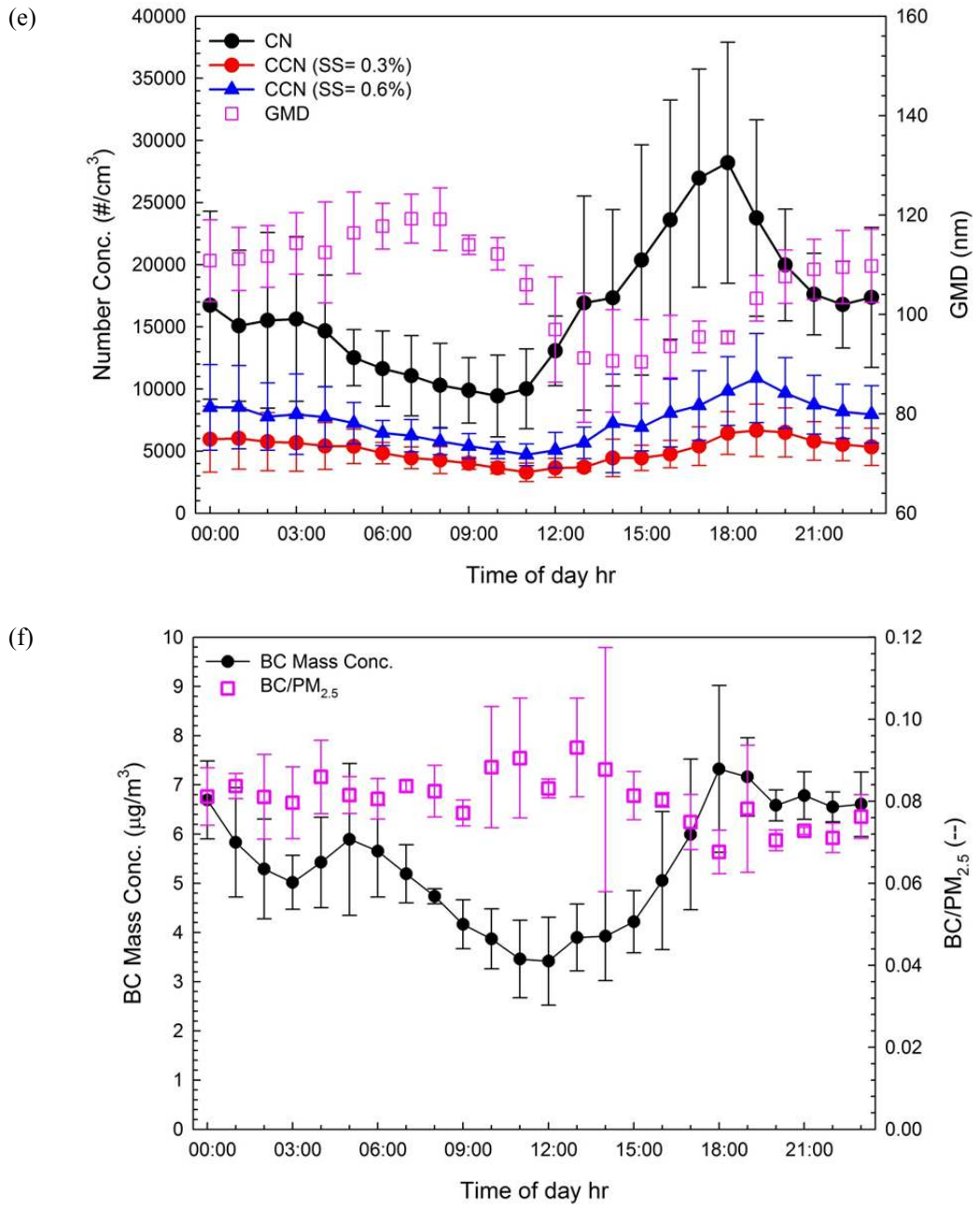

Fig. 6. (*continued*).

17–19, especially in the afternoon. In addition, the significant peak of UVBC and the collocated dip of the Delta-C diurnal curve observed routinely during 6:00 to 11:00 (local time) after March 17 may be the result of evaporation of semi-volatile OC due to dilution and/or photochemical reactions with less quantities of fresh BB aerosol in the morning. In short over the Southeast Asian BB source regions, the observation of UVBC implied that organic chemistry could still play an imperative role here to CCN activity.

Fig. 8 shows the diurnal variations of the CCN's κ value. Both κ diurnal profiles before and after March 17 had a well-defined afternoon minimum, and the profile was relatively flat after March 17. Similar to the CN concentration, GMD, and BC mass concentration, the κ diurnal pattern was greatly affected by fire counts. The low κ values in the afternoon might be the result of the rising production of fresh BB aerosols from local BB activities. These low κ values from two different observation periods converged to 0.05, whereas κ values in the morning (4:00 to 12:00, local time) were very different. These different values might be due to mixing with transported or locally aged BB aerosols and/or photochemical aging; however, the relative strengths of these processes are different. In summary, the κ value before March 17 showed a more obvious diurnal variation, and overall average κ value decreased significantly from 0.128 ± 0.259 to 0.049 ± 0.032 after March 17 ($p < 0.001$, *t*-test).

In many studies, the reported size-resolved κ values generally increase with particle size. This increase was

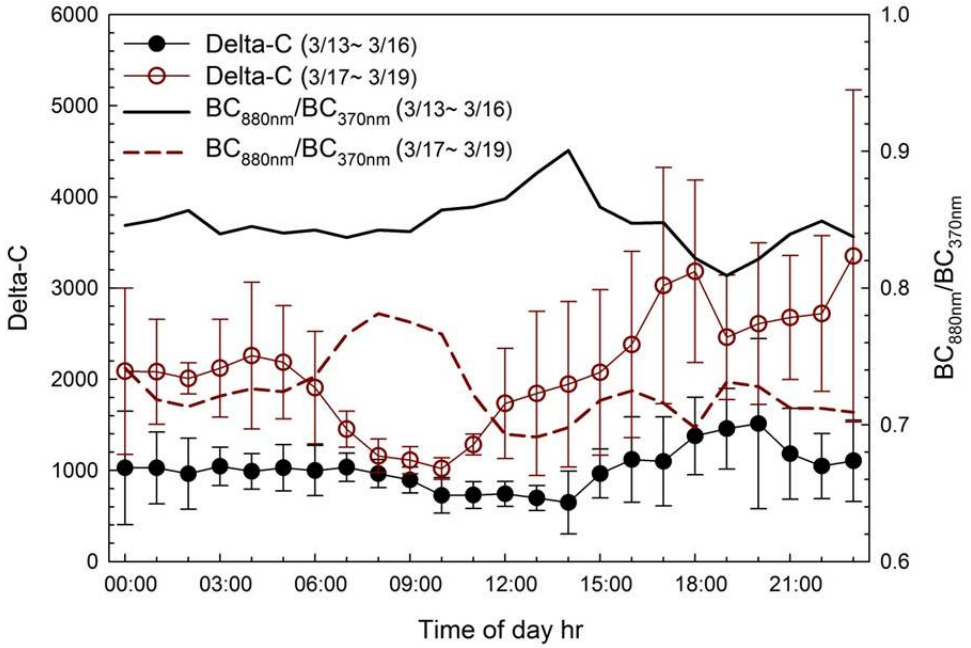

Fig. 7. Diurnal patterns of Delta-C (BC_{370nm}−BC_{880nm}) and BC_{880nm}/BC_{370nm} during March 13–16 and March 17–19.

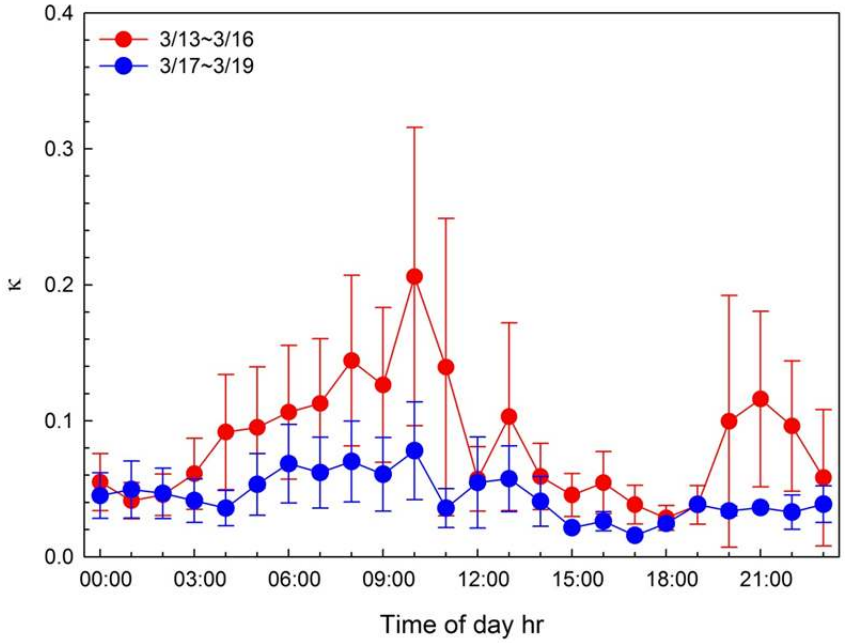

Fig. 8. Diurnal pattern of average κ values at five different SS levels during March 13–16 and March 17–19.

explained by the coating with more hygroscopic materials such as sulfate and nitrate during atmospheric transport and by the presence of more hydrophobic organics in the smaller particles (Gunthe *et al.*, 2009; Rose *et al.*, 2010; Hung *et al.*, 2014; Yue *et al.*, 2016). In other words, the chemical composition of CCN could be a function of particle size, especially after atmospheric transformation. Although the overall AR from DAK is strongly correlated with the GMD of a PSD, the κ values derived at different D_{act} values seem to be invariant (Fig. 9). Therefore, we suspect that the chemical compositions of CCN with different sizes in a BB source region are relatively homogeneous. The overall average κ (0.096) for the observation period before March 17 was very close to the κ value of SOA formed after photoaging (0.11), which was reported by Engelhart *et al.* (2012) in their UV chamber study. Thus, fractions of the BB aerosol measured before March 17 could undergo photochemical reactions. On the other hand, very low κ values (0.05) for different sizes after March 17 indicate that fresh BB aerosol in the source region was very hydrophobic. Coincidentally, we also observed the large fraction of UVBC and high Delta-C, which correlate well with the amount of

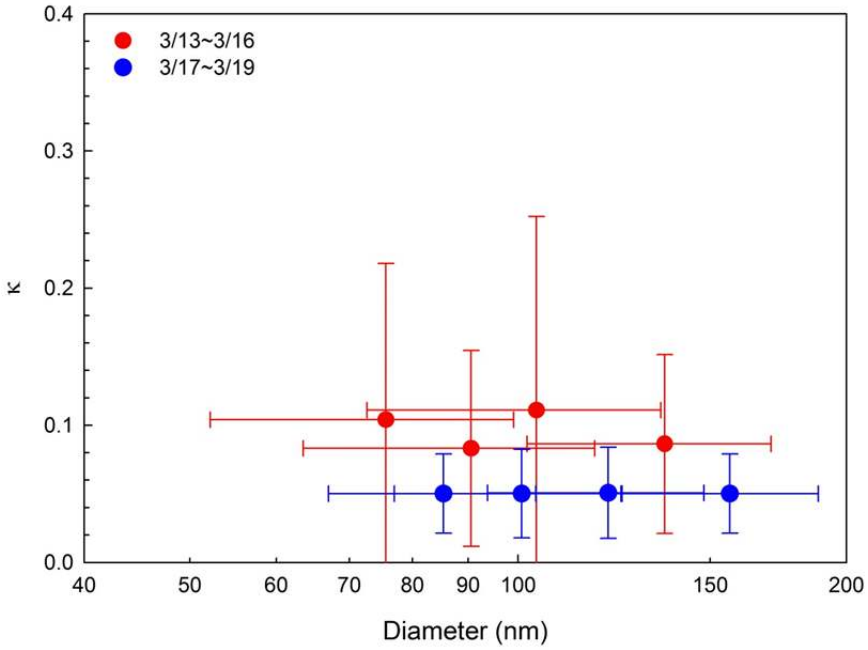

Fig. 9. κ values derived at different activation diameters.

particulate organic matter (*cf.* Fig. 7) (Carrico *et al.*, 2005). These findings are consistent with previous studies on water uptake of carbon-dominated aerosols (Petters *et al.*, 2009; Carrico *et al.*, 2010; Dusek *et al.*, 2011; Engelhart *et al.*, 2012).

To compare the CCN activities in different BB source regions, κ values measured in various field campaigns are summarized in Table 1. However, the κ-Köhler theory was proposed in 2007, and only the field studies after then reported κ values. Therefore, few κ values before 2007 summarized here are estimated based on their ground-based H-TDMA experimental results in the BB source regions. We found that, except those from the work of Rose *et al.* (2010) in Guangzhou (China), the κ values derived from ground-based observation of BB aerosols are generally less than 0.1. Furthermore, the very low κ values obtained in this study (0.05–0.08) agree well with those estimated from H-TDMA measurements (0.07–0.08) in the Amazonian region in Brazil (Rissler *et al.*, 2004, 2006). These very low κ values were attributed to the organic species dominating over the inorganic species that would be otherwise responsible for high hygroscopic growth factors. Rissler *et al.* further suggested that the relatively high molecular weight and the low degrees of dissociation of these organic compounds limit their water uptake, even though they could be water-soluble. Although detailed chemical characterization of CCN was not performed in this study, the large fraction of UVBC and high Delta-C derived through AE31 measurements could be supplemental indicators and could support this explanation.

Previous studies have indicated that BB pollutants are transported from Southeast Asia to South Asia by large-scale atmospheric circulation systems (Chen *et al.*, 2002). Recent studies further suggest that these pollutants may be transported downwind to the vicinity of Taiwan at high altitude (Wai *et al.*, 2008; Sheu *et al.*, 2010; Ou Yang *et al.*, 2012; Lin *et al.*, 2013). Therefore, the CCN ARs were monitored by the LABS concurrently with DAK during the observation period. On the basis of the backward trajectory analysis using the NOAA ARL HYbrid Single-Particle Lagrangian Integrated Trajectory (HYSPLIT) model v.4 ((Draxler and Rolph, 2003); HYSPLIT4 Model access via http://www.arl.noaa.gov/ready/hysplit4.html, Air Resour. Lab., Natl. Oceanic and Atmos. Admin., Silver Spring, MD.), there were two events affected by the long-range transport of BB aerosols from Southeast Asia (*cf.* Fig. S4). As seen in Fig. 10, the variation of AR at different SS values is less significant compared with that in the BB source region, especially in the high range of SS values. The different ARs in the BB source and receptor regions were observed only in the low range of SS values and only with lower AR values. The possible explanation for this finding is that the aged CCN in the high-AR ranges could already be activated and partially eliminated during long-range transport.

CONCLUSIONS

In this study, we intensively monitored the number concentrations of CCN and CN, the particle number size distributions at ambient conditions, and the mass concentrations of $PM_{2.5}$ and BC during the 2013 BASELInE campaign over northern SEA (DAK, Thailand). Cyclic particle growth from Aitken to accumulation sizes shortly after noontime was consistently observed (*cf.* S5). The CCN activity of BB aerosols in terms of AR and hygroscopicity (κ value) was further investigated in detail and analyzed with the diurnal variation of other variables such as fire counts, particle size, BC mass concentration, and Delta-C values. κ values in Southeast Asian BB source regions based on ground-based measurements are very rare and are valuable

Table 1. The hygroscopicity parameter κ of BB aerosols reported in previous studies.

Location	κ	Experimental Method	Reference
Canada	0.11 ± 0.04	CCNc, flight-based measurement	Lathem *et al.* (2013)
Guangzhou, China	0.24	CCNc, ground-based *in situ* measurement	Rose *et al.* (2010)
Balbina, Brazil	0.08[a]	H-TDMA, ground-based *in situ* measurement	Rissler *et al.* (2004)
Southwestern Amazonia, Brazil	0.07[a]	H-TDMA, ground-based *in situ* measurement	Rissler *et al.* (2006)
DAK, Thailand	0.08 ± 0.10 (3/13–16) 0.05 ± 0.03 (3/17–19)	CCNc, ground-based *in situ* measurement	This study

[a] The κ value was calculated from the growth factor by using the equation of Dusek *et al.* (2011).

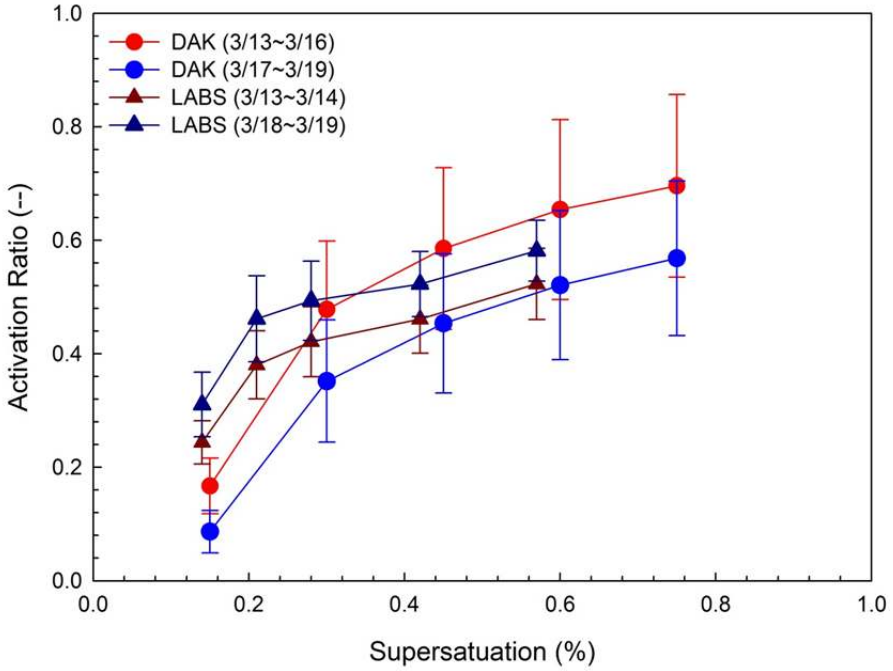

Fig. 10. Comparison of CCN activation ratios at DAK and LABS.

to global climate modeling studies and to studies on CCN. The findings in this study are as follows:

1. The aerosol properties measured near the BB source regions (CN, GMD, BC, AR, and κ values) have a strong diurnal pattern. This diurnal variation was directly related to the number of neighboring fire events and to cyclic changes in boundary layer thickness.
2. The AR before March 17 was 0.65 ± 0.16 (SS = 0.6%). It may be the result of BB aerosols mixing with transported aerosols or local photochemical aging of aerosols, which lead to large particle sizes (GMD = 125.7 ± 8.7 nm) and higher κ values (0.08 ± 0.10).
3. The AR after March 17 was 0.52 ± 0.13 (SS = 0.6%). It may be the result of fresh BB aerosols, which generally correlated with smaller particle sizes (GMD = 106.6 ± 9.5 nm) and demonstrated low hygroscopicity (κ = 0.05 ± 0.03).
4. A large fraction of UVBC (0.73 ± 0.02) and high Delta-C (2111.8 ± 632.4 ng m^{-3}) were observed after March 17. These suggest that the dominant, fresh BB aerosols respond to very low κ values.
5. The κ value in SEA near the source regions was low but comparable with previous values from CCN studies in other BB source regions (Table 1). Although detailed chemical analysis of BB aerosols was not performed, the AE31 measurements indicated that it could be attributed to the domination of organic species of aerosols in the BB source region.
6. The AR for BB events at the receptor site (LABS) did not change substantially compared with that for the BB source region. The aged CCN in the high-AR region could already be activated and partially eliminated during long-range transport.

ACKNOWLEDGMENTS

This work was supported by the National Science Council of Taiwan under grant no. NSC 102-2221-E-008-004-MY3 and by the Taiwan EPA under contracts no. EPA-103-U1L1-02-101 and EPA-102-FA11-03-A217. Deployment of 7-SEAS/BASELInE in Southeast Asia was supported by NASA Radiation Sciences Program, managed

by Dr. Hal B. Maring. We also thank all assistants from the region and many graduate students involved in the site operations, data analyses, and technical support for making the 7-SEAS/BASELInE campaign a success.

SUPPLEMENTARY MATERIALS

Supplementary data associated with this article can be found in the online version at http://www.aaqr.org.

REFERENCES

Adesina, A.J., Kumar, K.R. and Sivakumar, V. (2016). Aerosol-cloud-precipitation interactions over major cities in south Africa: Impact on regional environment and climate change. *Aerosol Air Qual. Res.* 16: 195–211.

Aiken, A.C., de Foy, B., Wiedinmyer, C., DeCarlo, P.F., Ulbrich, I.M., Wehrli, M.N., Szidat, S., Prevot, A.S.H., Noda, J., Wacker, L., Volkamer, R., Fortner, E., Wang, J., Laskin, A., Shutthanandan, V., Zheng, J., Zhang, R., Paredes-Miranda, G., Arnott, W.P., Molina, L.T., Sosa, G., Querol, X. and Jimenez, J.L. (2010). Mexico city aerosol analysis during MILAGRO using high resolution aerosol mass spectrometry at the urban supersite (T0) – Part 2: Analysis of the biomass burning contribution and the non-fossil carbon fraction. *Atmos. Chem. Phys.* 10: 5315–5341.

Anderson, B.E., Grant, W.B., Gregory, G.L., Browell, E.V., Collins, J.E., Sachse, G.W., Bagwell, D.R., Hudgins, C.H., Blake, D.R. and Blake, N.J. (1996). Aerosols from Biomass burning over the tropical South Atlantic region: Distributions and impacts. *J. Geophys. Res.* 101: 24117–24137.

Andreae, M.O., Rosenfeld, D., Artaxo, P., Costa, A.A., Frank, G.P., Longo, K.M. and Silva-Dias, M.A.F. (2004). Smoking rain clouds over the Amazon. *Science* 303: 1337–1342.

Andreae, M.O. and Rosenfeld, D. (2008). Aerosol–cloud–precipitation interactions. Part 1. The nature and sources of cloud-active aerosols. *Earth Sci. Rev.* 89: 13–41.

Bates, T.S., Anderson, T.L., Baynard, T., Bond, T., Boucher, O., Carmichael, G., Clarke, A., Erlick, C., Guo, H. and Horowitz, L. (2006). Aerosol direct radiative effects over the northwest Atlantic, northwest Pacific, and north Indian Oceans: estimates based on in-situ chemical and optical measurements and chemical transport modeling. *Atmos. Chem. Phys.* 6:1657–1732.

Bhawar, R.L. and Rahul, P.R.C. (2013). Aerosol-cloud-interaction variability induced by atmospheric brown clouds during the 2009 Indian summer monsoon drought. *Aerosol Air Qual. Res.* 13: 1384–1391.

Carrico, C.M., Kreidenweis, S.M., Malm, W.C., Day, D.E., Lee, T., Carrillo, J., McMeeking, G.R. and Collett, J.L. (2005). Hygroscopic growth behavior of a carbon-dominated aerosol in Yosemite National Park. *Atmos. Environ.* 39: 1393–1404.

Carrico, C.M., Petters, M.D., Kreidenweis, S.M., Sullivan, A.P., McMeeking, G.R., Levin, E.J.T., Engling, G., Malm, W.C. and Collett Jr, J.L. (2010). Water uptake and chemical composition of fresh aerosols generated in open burning of biomass. *Atmos. Chem. Phys.* 10: 5165–5178.

Chen, T.C., Yen, M.C., Huang, W.R. and Gallus Jr, W.A. (2002). An east Asian cold surge: Case study. *Mon. Weather Rev.* 130: 2271–2290.

Clarke, A., McNaughton, C., Kapustin, V., Shinozuka, Y., Howell, S., Dibb, J., Zhou, J., Anderson, B., Brekhovskikh, V. and Turner, H. (2007). Biomass burning and pollution aerosol over North America: Organic components and their influence on spectral optical properties and humidification response. *J. Geophys. Res.* 112: D12S18.

Corrigan, C.E., Ramanathan, V. and Schauer, J.J. (2006). Impact of monsoon transitions on the physical and optical properties of aerosols. *J. Geophys. Res.* 111: D18208.

Crutzen, P.J. and Andreae, M.O. (1990). Biomass burning in the tropics: Impact on atmospheric chemistry and biogeochemical cycles. *Science* 250:1669–1678.

Dinh, V.P., Lacaux, J.P. and Serpolay, R. (1992). Cloud forming properties of biomass burning aerosols, In *Nucleation and Atmospheric Aerosols*, Fukuta, N. and Wagner, P.E. (Eds.), Deepak Publishing, New York, pp. 173–176.

Draxler, R.R. and Rolph, G.D. (2003). HYSPLIT (HYbrid Single-Particle Lagrangian Integrated Trajectory) Model Access via NOAA ARL READY website (http://www.arl.noaa.gov/ready/hysplit4.html). NOAA Air Resources Laboratory, Silver Spring, Md.

Duncan, B.N., Martin, R.V., Staudt, A.C., Yevich, R. and Logan, J.A. (2003). Interannual and seasonal variability of biomass burning emissions constrained by satellite observations. *J. Geophys. Res.* 108: ACH 1-1–ACH 1-22.

Dusek, U., Frank, G. P., Massling, A., Zeromskiene, K., Iinuma, Y., Schmid, O., Helas, G., Hennig, T., Wiedensohler, A. and Andreae, M.O. (2011). Water uptake by biomass burning aerosol at sub-and supersaturated conditions: Closure studies and implications for the role of organics. *Atmos. Chem. Phys.* 11: 9519–9532.

Engelhart, G.J., Hennigan, C.J., Miracolo, M.A., Robinson, A.L. and Pandis, S.N. (2012). Cloud condensation nuclei activity of fresh primary and aged biomass burning aerosol. *Atmos. Chem. Phys.* 12: 7285–7293.

Gunthe, S.S., King, S.M., Rose, D., Chen, Q., Roldin, P., Farmer, D.K., Jimenez, J.L., Artaxo, P., Andreae, M.O. and Martin, S.T. (2009). Cloud condensation nuclei in pristine tropical rainforest air of amazonia: Size-resolved measurements and modeling of atmospheric aerosol composition and CCN activity. *Atmos. Chem. Phys.* 9: 7551–7575.

Hallett, J., Hudson, J.G. and Rogers, C.F. (1989). Characterization of combustion aerosols for haze and cloud formation. *Aerosol Sci. Technol.* 10: 70–83.

Haywood, J.M., Osborne, S.R., Francis, P.N., Keil, A., Formenti, P., Andreae, M.O. and Kaye, P.H. (2003). The mean physical and optical properties of regional haze dominated by biomass burning aerosol measured from the C-130 aircraft during SAFARI 2000. *J. Geophys. Res.* 108: 8473.

Heil, A. and Goldammer, J. (2001). Smoke-haze pollution: A review of the 1997 episode in Southeast Asia. *Reg. Environ. Change* 2: 24–37.

Hung, H.M., Lu, W.J., Chen, W.N., Chang, C.C., Chou, C.K. and Lin, P.H. (2014). Enhancement of the hygroscopicity parameter kappa of rural aerosols in northern Taiwan by anthropogenic emissions. *Atmos. Environ.* 84: 78–87.

Jeong, C.H., Hopke, P.K., Kim, E. and Lee, D.W. (2004). The comparison between thermal-optical transmittance elemental carbon and aethalometer black carbon measured at multiple monitoring sites. *Atmos. Environ.* 38: 5193–5204.

Kumar, M., Lipi, K., Sureshbabu, S., Mahanti, N.C. (2011). Aerosol properties over Ranchi measured from aethalometer. *Atmos. Clim. Sci.* 1: 91–94.

Lathem, T.L., Beyersdorf, A.J., Thornhill, K.L., Winstead, E.L., Cubison, M.J., Hecobian, A., Jimenez, J.L., Weber, R.J., Anderson, B.E. and Nenes, A. (2013). Analysis of CCN activity of Arctic aerosol and Canadian biomass burning during summer 2008. *Atmos. Chem. Phys.* 13: 2735–2756.

Le Canut, P., Andreae, M.O., Harris, G.W., Wienhold, F.G. and Zenker, T. (1996). Airborne studies of emissions from savanna fires in southern Africa: 1. Aerosol emissions measured with a laser optical particle counter. *J. Geophys. Res.* 101: 23615–23630.

Levine, J.S. Ed. (1996). *Biomass Burning and Global Change*, MIT, Cambridge, MA.

Lin, N.H., Tsay, S.C., Maring, H.B., Yen, M.C., Sheu, G.R., Wang, S.H., Chi, K.H., Chuang, M.T., Ou-Yang, C.F., Fu, J.S., Reid, J.S., Lee, C.T., Wang, L.C., Wang, J.L., Hsu, C.N., Sayer, A.M., Holben, B.N., Chu, Y.C., Nguyen, X.A., Sopajaree, K., Chen, S.J., Cheng, M.T., Tsuang, B.J., Tsai, C.J., Peng, C.M., Schnell, R.C., Conway, T., Chang, C.T., Lin, K.S., Tsai, Y.I., Lee, W.J., Chang, S.C., Liu, J.J., Chiang, W.L., Huang, S.J., Lin, T.H. and Liu, G.R. (2013). An overview of regional experiments on biomass burning aerosols and related pollutants in Southeast Asia: From BASE-ASIA and the dongsha experiment to 7-SEAS. *Atmos. Environ.* 78: 1–19.

Lin, N.H., Sayer, A.M., Wang, S.H., Loftus, A.M., Hsiao, T.C., Sheu, G.R., Hsu, N.C., Tsay, S.C. and Chantara, S. (2014). Interactions between biomass-burning aerosols and clouds over Southeast Asia: Current status, challenges, and perspectives. *Environ. Pollut.* 195: 292–307.

Martin, S.T. (2000). Phase transitions of aqueous atmospheric particles. *Chem. Rev.* 100: 3403–3454.

Ou Yang, C.F., Lin, N.H., Sheu, G.R., Lee, C.T. and Wang, J.L. (2012). Seasonal and diurnal variations of ozone at a high-altitude mountain baseline station in East Asia. *Atmos. Environ.* 46: 279–288.

Pani, S.K., Wang, S.H., Lin, N.H., Tsay, S.C., Lolli, S., Chuang, M.T., Lee, C.T., Chantara, S. and Yu, J.Y. (2016a). Assessment of aerosol optical property and radiative effect for the layer decoupling cases over the northern South China Sea during the 7-SEAS/Dongsha Experiment. *J. Geophys Res. Atmos.* 121: 4894–4906.

Pani, S.K., Wang, S.H., Lin, N.H., Lee, C.T., Tsay, S.C., Holben, B.N., Janjai, S., Hsiao, T.C., Chuang, M.T. and Chantara, S. (2016b). Radiative effect of springtime biomass-burning aerosols over Northern Indochina during 7-SEAS/BASELInE 2013 campaign. *Aerosol Air Qual. Res.* 16: 2802–2817.

Park, K., Chow, J.C., Watson, J.G., Trimble, D.L., Doraiswamy, P., Park, K., Arnott, W.P., Stroud, K.R., Bowers, K. and Bode, R. (2006). Comparison of continuous and filter-based carbon measurements at the fresno supersite. *J. Air Waste Manage. Assoc.* 56: 474–491.

Petters, M.D. and Kreidenweis, S.M. (2007). A single parameter representation of hygroscopic growth and cloud condensation nucleus activity. *Atmos. Chem. Phys.* 7: 1961–1971.

Petters, M.D., Carrico, C.M., Kreidenweis, S.M., Prenni, A.J., DeMott, P.J., Collett, J.L. and Moosmueller, H. (2009). Cloud condensation nucleation activity of biomass burning aerosol. *J. Geophys. Res.* 114: D22205.

Pierce, J.R., Chen, K. and Adams, P.J. (2007). Contribution of primary carbonaceous aerosol to cloud condensation nuclei: Processes and uncertainties evaluated with a global aerosol microphysics model. *Atmos. Chem. Phys.* 7: 5447–5466.

Posfai, M., Simonics, R., Li, J., Hobbs, P.V. and Buseck, P.R. (2003). Individual aerosol particles from biomass burning in Southern Africa: 1. Compositions and size distributions of carbonaceous particles. *J. Geophys. Res.* 108: 8483.

Pratt, K.A., Murphy, S.M., Subramanian, R., DeMott, P.J., Kok, G.L., Campos, T., Rogers, D.C., Prenni, A.J., Heymsfield, A.J. and Seinfeld, J.H. (2011). Flight-based chemical characterization of biomass burning aerosols within two prescribed burn smoke plumes. *Atmos. Chem. Phys.* 11: 12549–12565.

Reid, J.S. and Hobbs, P.V. (1998). Physical and optical properties of young smoke from individual biomass fires in Brazil. *J. Geophys. Res.* 103: 32013–32030.

Reid, J.S., Hobbs, P.V., Ferek, R.J., Blake, D.R., Martins, J.V., Dunlap, M.R. and Liousse, C. (1998). Physical, chemical, and optical properties of regional hazes dominated by smoke in Brazil. *J. Geophys. Res.* 103: 32059–32080.

Reid, J.S., Koppmann, R., Eck, T.F. and Eleuterio, D.P. (2005). A review of biomass burning emissions Part II: Intensive physical properties of biomass burning particles. *Atmos. Chem. Phys.* 5: 799–825.

Reutter, P., Su, H., Trentmann, J., Simmel, M., Rose, D., Gunthe, S.S., Wernli, H., Andreae, M.O. and Pöschl, U. (2009). Aerosol-and updraft-limited regimes of cloud droplet formation: Influence of particle number, size and hygroscopicity on the activation of cloud condensation nuclei (CCN). *Atmos. Chem. Phys.* 9: 7067–7080.

Rissler, J., Swietlicki, E., Zhou, J., Roberts, G., Andreae, M.O., Gatti, L.V. and Artaxo, P. (2004). Physical properties of the sub-micrometer aerosol over the Amazon rain forest during the wet-to-dry season transition-comparison of modeled and measured CCN concentrations. *Atmos.*

Chem. Phys. 4: 2119–2143.

Rissler, J., Vestin, A., Swietlicki, E., Fisch, G., Zhou, J., Artaxo, P. and Andreae, M.O. (2006). Size distribution and hygroscopic properties of aerosol particles from dry-season biomass burning in Amazonia. *Atmos. Chem. Phys.* 6: 471–491.

Rose, D., Nowak, A., Achtert, P., Wiedensohler, A., Hu, M., Shao, M., Zhang, Y., Andreae, M.O. and Pöschl, U. (2010). Cloud condensation nuclei in polluted air and biomass burning smoke near the mega-city Guangzhou, China–Part 1: Size-resolved measurements and implications for the modeling of aerosol particle hygroscopicity and CCN activity. *Atmos. Chem. Phys.* 10: 3365–3383.

Sandradewi, J., Prévôt, A.S.H., Alfarra, M.R., Szidat, S., Wehrli, M.N., Ruff, M., Weimer, S., Lanz, V.A., Weingartner, E. and Perron, N. (2008). Comparison of several wood smoke markers and source apportionment methods for wood burning particulate Mass. *Atmos. Chem. Phys. Discuss.* 8: 8091–8118.

Sayer, A.M., Hsu, N.C., Hsiao, T.C., Pantina, P., Kuo, F., Ou-Yang, C.F., Holben, B.N., Janjai, S., Chantara, S., Wang, S.H., Loftus, A.M., Lin, N.H. and Tsay, S.C. (2016). In-situ and remotely-sensed observations of biomass burning aerosols at Doi Ang Khang, Thailand during 7-SEAS/BASELInE 2015. *Aerosol Air Qual. Res.* 16: 2786–2801.

See, S.W., Balasubramanian, R. and Wang, W. (2006). A study of the physical, chemical, and optical properties of ambient aerosol particles in Southeast Asia during hazy and nonhazy days. *J. Geophys. Res.* 111: D10S08.

Sheu, G.R., Lin, N.H., Wang, J.L., Lee, C.T., Ou Yang, C.F. and Wang, S.H. (2010). Temporal distribution and potential sources of atmospheric mercury measured at a high-elevation background station in Taiwan. *Atmos. Environ.* 44: 2393–2400.

Spracklen, D.V., Carslaw, K.S., Pöschl, U., Rap, A. and Forster, P.M. (2011). Global cloud condensation nuclei influenced by carbonaceous combustion aerosol. *Atmos. Chem. Phys.* 11: 9067–9087.

Streets, D.G., Yarber, K.F., Woo, J.H. and Carmichael, G.R. (2003). Biomass burning in Asia: Annual and seasonal estimates and atmospheric emissions. *Global Biogeochem. Cycles* 17: 1099.

Tsay, S.C., Hsu, C.N., Lau, W.K.M., Li, C., Gabriel, P.M., Ji, Q., Holben, B.N., Welton, E.J., Nguyen, X.A., Janjia, S., Lin, N.H., Reid, J.S., Boonjawat, J., Howell, S.G., Huebert, B.J., Fu, J.S., Hansell, R.A., Sayer, A.M., Gautam, R., Wang, S.H., Goodloe, C.S., Miko, L.R., Shu, P.K., Loftus, A.M., Huang, J., Kim, J.Y., Jeong, M.J. and Pantina, P. (2013). From BASE-ASIA toward 7-SEAS: A satellite-surface perspective of boreal spring biomass-burning aerosols and clouds in Southeast Asia. *Atmos. Environ.* 78: 20–34.

Tsay, S.C., Maring, H.B., Lin, N.H., Buntoung, S., Chantara, S., Chuang, H.C., Gabriel, P.M., Goodloe, C.S., Holben, B.N., Hsiao, T.C., Hsu, N.C., Janjai, S., Lau, W.K.M., Lee, C.T., Lee, J., Loftus, A.M., Nguyen, A.X., Nguyen, C.M., Pani, S.K., Pantina, P., Sayer, A.M., Tao, W.K., Wang, S.H., Welton, E.J., Wiriya, W. and Yen, M.C. (2016). Satellite-surface perspectives of air quality and aerosol-cloud effects on the environment: An overview of 7-SEAS/BASELInE. *Aerosol Air Qual. Res.* 16: 2581–2602.

Wai, K.M., Lin, N.H., Wang, S.H. and Dokiya, Y. (2008). Rainwater chemistry at a high-altitude Station, Mt. Lulin, Taiwan: Comparison with a background station, Mt. Fuji. *J. Geophys. Res.* 113: D06305.

Wang, S.H., Welton, E.J., Holben, B.N., Tsay, S.C., Lin, N.H., Giles, D., Stewart, S.A., Janjai, S., Nguyen, X.A., Hsiao, T.C., Chen, W.N., Lin, T.H., Buntoung, S., Chantara, S. and Wiriya, W. (2015). Vertical distribution and columnar optical properties of springtime biomass-burning aerosols over Northern Indochina during 2014 7-SEAS campaign. *Aerosol Air Qual. Res.* 15: 2037–2050.

Wang, Y., Hopke, P.K., Rattigan, O.V. and Zhu, Y. (2011). Characterization of ambient black carbon and wood burning particles in two urban areas. *J. Environ. Monit.* 13: 1919–1926.

Wardoyo, A.Y.P., Morawska, L., Ristovski, Z.D., Jamriska, M., Carr, S. and Johnson, G. (2007). Size distribution of particles emitted from grass fires in the Northern Territory, Australia. *Atmos. Environ.* 41: 8609–8619.

Yu, G.H., Cho, S.Y., Bae, M.S. and Park, S.S. (2014). Difference in production routes of water-soluble organic carbon in $PM_{2.5}$ observed during non-biomass and biomass burning periods in Gwangju, Korea. *Environ. Sci. Processes Impacts* 16: 1726–1736.

Yue, D., Zhong, L., Zhang, T., Shen, J., Yuan, L., Ye, S., Zhou, Y. and Zeng, L. (2016). Particle growth and variation of cloud condensation nucleus activity on polluted days with new particle formation: A case study for regional air pollution in the PRD region, China. *Aerosol Air Qual. Res.* 16: 323–335.

Received for review, July 13, 2015
Revised, November 6, 2015
Accepted, November 9, 2015